

Coherent pion production in neutrino (anti-neutrino)-nucleus interaction

Hariom Sogarwal, Prashant Shukla*

Nuclear Physics Division, Bhabha Atomic Research Centre, Mumbai 400085, India

Homi Bhabha National Institute, Anushakti Nagar, Mumbai 400094, India

Abstract

We present a study of coherent pion production in neutrino-nucleus interactions using the formalism based on partially conserved axial current theorem which connects the neutrino-nucleus cross section to the pion-nucleus elastic scattering cross section. Pion-nucleus elastic scattering cross section is calculated using Glauber model which takes three inputs, nuclear densities, pion-nucleon cross section and $\alpha_{\pi N}$ which is the ratio of real to imaginary part of πN forward scattering amplitude, for which the parametrizations are obtained from measured data. We calculate the differential and integrated cross sections for charge and neutral current coherent pion production in neutrino (anti-neutrino)-nucleus scattering for a range of nuclear targets from light to heavy materials such as lithium, carbon, hydrocarbon, oxygen, silicon, argon, iron and lead. The results of these cross section calculations are compared with the measured data and with the calculations from the Berger-Sehgal model and GENIE package. There is an excellent agreement between the calculated and measured cross sections with Glauber model. While GENIE and Berger-Sehgal model give a good description of the data in the lower energy range the present calculations describe the data in all energy ranges. Predictions are also made for upcoming experiments like INO and DUNE in the coherent region of neutrino cross section.

*Corresponding author

Email address: pshuklabarc@gmail.com (Prashant Shukla)

Keywords: Coherent pion production, Neutrino-nucleus interactions, Glauber model, PCAC, GENIE

1. Introduction

The neutrinos produced in upper atmosphere and in accelerators are used for studying the phenomena of neutrino oscillations by many experiments worldwide [1, 2, 3]. Most experiments focussing on muon neutrinos are designed to measure recoil muons when neutrinos undergo charge current interaction in the detector medium. Some examples of detector media are; iron in case of India-based Neutrino Observatory (INO) [4] and argon in case of DUNE experiment [5]. Bulk of the interactions in the detector comes from intermediate energy neutrinos having contribution from many processes which include quasi elastic scattering, interaction via resonance pion production and deep inelastic scattering [6, 7, 8]. One of the important processes in the resonance production region is coherent pion production in which the nucleus interacts as a whole with the neutrino with its quantum state remains unchanged. The charge current (CC) and neutral current (NC) coherent pion production processes are given as

$$\nu_\mu + A \rightarrow \mu^- + \pi^+ + A. \text{ (CC)}$$

$$\nu_\mu + A \rightarrow \nu_\mu + \pi^0 + A. \text{ (NC)}$$

The four-momentum transfer Q between the incoming neutrino and outgoing lepton is given by $Q^2 = -q^2 = \mathbf{q}^2 - \nu^2$. Here, \mathbf{q} is the 3-momentum transfer and $\nu (= E_\nu - E_\mu)$ is the energy difference between the incident neutrino (with energy E_ν) and outgoing lepton (with energy E_μ). For coherent pion production, the squared momentum transfer to the nucleus from the lepton-pion system $|t| = |(q - p_\pi)^2|$ remains small. Here p_π is the 4-momentum of outgoing pion. Estimating coherent pion production is important for the analysis of data of neutrino oscillation experiments. The simplest theoretical approach for describing coherent pion production is based on Adler's Partially Conserved Axial Current (PCAC) theorem which relates the neutrino induced coherent

pion production to the pion-nucleus elastic scattering [9, 10, 11, 12, 13, 14]. The PCAC model has been successful in describing coherent pion production at high energy [9]. Work with the same assumption has been used at low energy in Ref. [12]. There are several microscopic models as well for coherent scattering e.g. in Refs. [15, 16, 17, 18]. The GENIE (**G**enerates **E**vents for **N**eutrino **I**nteraction **E**xperiments) [19] uses PCAC theorem with Rein-Sehgal model [9] for the coherent neutrino-nucleus scattering which results in the production of forward going pions in both charge current and neutral current interactions.

To obtain the elastic pion-nucleus scattering cross section, the Berger-Sehgal (BS) model [13] is used in literature which basically follows Rein-Sehgal (RS) method [9] with some improvement in the way parametrizations are done for elementary cross sections. In this model, the elastic scattering pion nucleus cross section is obtained from measured total and elastic pion nucleon cross sections. Further an exponential function is assumed for t dependence of elastic scattering cross section and attenuation of pion is made dependent on nuclear size. GENIE uses RS model and its difference with BS calculations can arise due to input elementary cross sections and other input parameters. The work presented in Ref. [20] calculates the pion-nucleus elastic scattering cross section using the Glauber model in terms of measured nuclear densities and measured pion nucleon cross sections. In view of the recent data at various energies we aim to revisit this model and improve the treatment of input parameters namely total pion nucleon cross sections, $\alpha_{\pi N}$ (the ratio of real to imaginary part of forward scattering amplitude) and nuclear density function parameters. The parametrizations of the total pion nucleon cross sections have been done and presented using the latest data. The values of $\alpha_{\pi N}$ obtained with the elementary scattering amplitudes may change when one applies the formalism to nuclear targets and are typically around one [38]. In view of this, we use the pion nucleus elastic scattering differential cross section data available for few incident energies of pions on a broad range of nuclear targets to obtain $\alpha_{\pi N}$. We also compare with the Berger-Sehgal model which gives reasonable description of elastic scattering differential cross section at lower scattering angles only. Re-

cently, charge and neutral current coherent pion production has been measured for several nuclei by many experiments such as MINER ν A [21, 22], CHARM-II [23], Aachen-Padova [24], Gargamelle [25], CHARM [26], SKAT [27], NOMAD [28], 15'B.C. [29], SciBooNE [30], MINOS [31], NO ν A [32], K2K [33], T2K[34, 35] and MiniBooNE [36]. The comparison of Glauber approach has been done with the calculations from Berger-Sehgal (BS) model and the GENIE package (version v3_00_06a).

In this work, we calculate coherent pion production in neutrino-nucleus interactions in the resonance region using the PCAC based formalism. Pion-nucleus elastic scattering cross section is calculated with the Glauber model using pion-nucleon cross section and $\alpha_{\pi N}$. The parametrizations of latest measured total pion nucleon cross section has been presented. We calculate the differential and integrated cross sections for charge and neutral current coherent pion production in neutrino (anti-neutrino)-nucleus scattering for a range of nuclear targets: lithium, carbon, hydrocarbon, scintillator, oxygen, silicon, argon, iron, and lead using the model with fixed parameters. The results of these cross section calculations are compared with the measured data, BS model and GENIE package.

2. The formulation of the model

The differential cross section for the charge current coherent pion production scattering process [10, 13] is

$$\frac{d\sigma^{CC}}{dQ^2 d\nu d|t|} = \frac{G_F^2 \cos^2 \theta_C f_\pi^2 uv}{2\pi^2 |\mathbf{q}|} \left[\left(G_A - \frac{1}{2} \frac{Q_m^2}{(Q^2 + m_\pi^2)} \right)^2 + \frac{\nu}{4E_\nu} (Q^2 - Q_m^2) \frac{Q_m^2}{(Q^2 + m_\pi^2)^2} \right] \times \frac{d\sigma(\pi A \rightarrow \pi A)}{d|t|}. \quad (1)$$

For the neutral current, the above expression is modified as

$$\frac{d\sigma^{NC}}{dQ^2 d\nu d|t|} = \frac{G_F^2 f_\pi^2 G_A^2}{4\pi^2 |\mathbf{q}|} u v \times \frac{d\sigma(\pi A \rightarrow \pi A)}{d|t|}. \quad (2)$$

Here $G_F (=1.16639 \times 10^{-5} \text{ GeV}^{-2})$ is the Fermi coupling constant and $\cos \theta_C (=0.9725)$. The kinematic factors u and v are given by : $u, v = (E_\nu + E_\mu \pm |\mathbf{q}|)/(2 E_\nu)$.

The pion decay constant is f_π ($= 0.93 m_\pi$) and $d\sigma(\pi A \rightarrow \pi A)/d|t|$ is the pion-nucleus differential elastic cross section calculated assuming ν as the total incident energy of pion in laboratory frame. The axial vector form factor can be defined as $G_A = m_A^2/(Q^2 + m_A^2)$ [13] with the axial vector meson mass m_A ($= 1.05 \text{ GeV}/c^2$) [7]. The high energy approximation to the true minimal Q^2 is given by $Q_m^2 = m_l^2 \nu/(E_\nu - \nu)$, where m_l is the mass of outgoing lepton which will be muon mass in case of CC. The expression for neutral current (NC) (Eq. 2) is obtained from Eq. 1 by putting $m_l=0$, $\theta_C=0$ and divide the right hand side of the Eq. 1 by 2, because $f_{\pi^0} = f_\pi/\sqrt{2}$.

The kinematic limits are guided by the work in Ref. [12]. The upper limit of Q^2 is taken as 1.0 GeV^2 . The ν integration should be done in the range $\max(\xi\sqrt{Q^2}, \nu_{\min}) < \nu < \nu_{\max}$. In the previous work [20] the calculations were performed at two values of ξ ($=1,2$). In the present work, we include this variation as uncertainty in both Glauber and BS calculations.

Pion-nucleus differential cross section

To obtain the elastic pion-nucleus scattering cross section, the Berger-Sehgal (BS) model [13] is used in literature which basically follows Rein-Sehgal (RS) method [9]. In their model, the pion-nucleus elastic scattering cross section is obtained from measured total pion nucleon cross sections. Further an exponential function is assumed for t dependence and the attenuation of pions is made dependent on nuclear radius. We use scattering theory to obtain the pion-nucleus differential elastic cross section given as

$$\frac{d\sigma_{el}}{d|t|} = \frac{\pi}{k^2} |f(t)|^2, \quad (3)$$

where $f(t)$ is given by

$$f(t) = \frac{1}{2ik} \sum_{l=0}^{\infty} (2l+1) (S_l - 1) P_l(\cos\theta). \quad (4)$$

Here $t = -4k^2 \sin^2 \theta/2$ and k is the momentum of pion and θ is the scattering angle of pion in center of mass frame.

We use the Glauber model to obtain the scattering matrix S_l in terms of pion-nucleus impact parameter b by [37]

$$S_l = \exp(i\chi(b)), \quad bk = \left(l + \frac{1}{2}\right), \quad (5)$$

The Glauber phase shift $\chi(b)$ is given by

$$\chi(b) = \frac{1}{2}\sigma_{\pi N}(\alpha_{\pi N} + i)AT(b) \quad (6)$$

Here $\sigma_{\pi N}$ is the average total pion-nucleon cross section and $\alpha_{\pi N}$ is the ratio of real to imaginary part of the πN forward scattering amplitude. $T(b)$ is the overlap function obtained by the Glauber model, the full details of which are given in Ref. [20]. The pion-nucleon cross sections are taken from the Particle Data Group [3].

Figure 1 (a) and (b) show the measured total cross sections for π^+p and π^-p collisions respectively as a function of pion momentum in laboratory frame. The data is fitted with Breit-Wigners and Regge function for pion momentum up to 4 GeV/ c and a pure Regge function above 4 GeV/ c . The Regge term above 4 GeV/ c is given by $25.06 - 15.16/\sqrt{p_\pi} + 41.07\sqrt{p_\pi}$ for π^+p case and $24.73 - 6.91/\sqrt{p_\pi} + 37.37\sqrt{p_\pi}$ for π^-p case.

The values of $\alpha_{\pi N}$ obtained with the elementary scattering amplitudes may change when one applies the formalism to nuclear targets and are typically around one [38]. In view of this, we use the pion nucleus elastic scattering data available for few incident energies of pions on a broad range of nuclear targets to obtain $\alpha_{\pi N}$.

Figure 2 shows pion- ^{12}C elastic scattering differential cross section as function of pion scattering angle at three pion kinetic energies of 400 MeV, 500 MeV and 675.5 MeV scaled respectively by factors 1000, 10 and 0.1 [39, 40]. The blue bands are obtained using the Glauber model for $\alpha_{\pi N} = 0.9-1.4$ and dashed lines are the calculations of the Berger-Sehgal model [13].

Figure 3 shows pion- ^{40}Ca elastic scattering differential cross section as function of pion scattering angle at three pion kinetic energies of 400 MeV, 500 MeV and 675.5 MeV scaled respectively by factors 1000, 10 and 0.1 [39, 40]. The blue

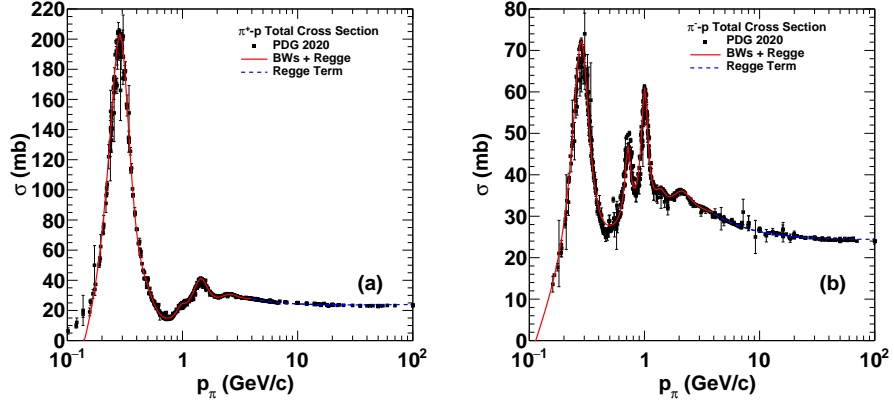


Figure 1: Measured total cross sections for (a) π^+p and (b) π^-p collisions as a function of pion momentum along with the fit function.

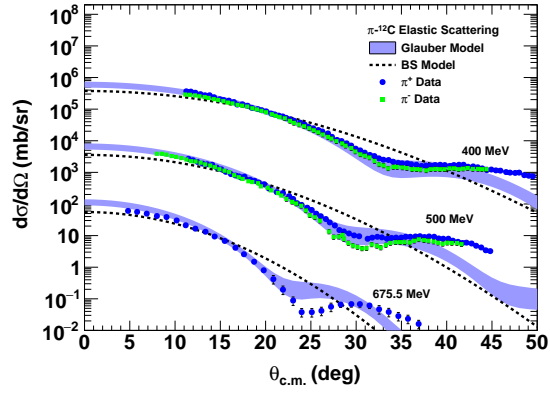


Figure 2: Pion- ^{12}C elastic scattering differential cross section as function of pion scattering angle at three pion kinetic energies of 400 MeV, 500 MeV and 675.5 MeV scaled respectively by factors 1000, 10 and 0.1 [39, 40]. The blue bands are obtained using the Glauber model for $\alpha_{\pi N} = 0.9-1.4$ and dashed lines are the calculations of the Berger-Sehgal (BS) model [13].

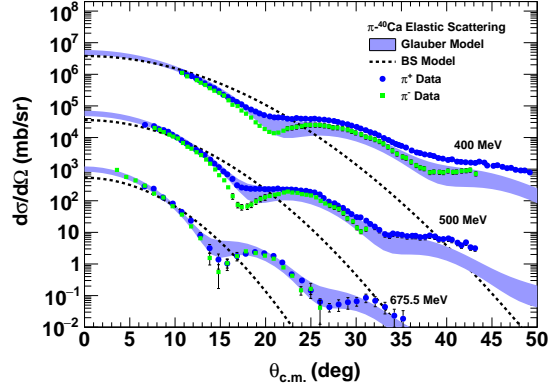


Figure 3: Pion- ^{40}Ca elastic scattering differential cross section as function of pion scattering angle at three pion kinetic energies of 400 MeV, 500 MeV and 675.5 MeV scaled respectively by factors 1000, 10 and 0.1 [39, 40]. The blue bands are obtained using the Glauber model for $\alpha_{\pi N} = 0.9-1.4$ and dashed lines are the calculations of the Berger-Sehgal model [13].

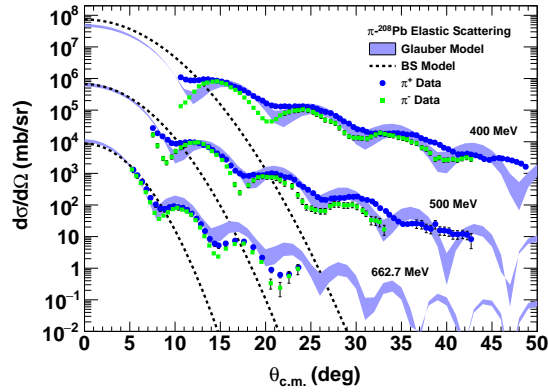


Figure 4: Pion- ^{208}Pb elastic scattering differential cross section as function of pion scattering angle at three pion kinetic energies of 400 MeV, 500 MeV and 662.7 MeV scaled respectively by factors 1000, 10 and 0.1 [39, 40]. The blue bands are obtained using the Glauber model for $\alpha_{\pi N} = 0.9-1.4$ and dashed lines are the calculations of the Berger-Sehgal model [13].

bands are obtained using the Glauber model for $\alpha_{\pi N} = 0.9-1.4$ and dashed lines are the calculations of the Berger-Sehgal model [13].

Figure 4 shows pion- ^{208}Pb elastic scattering differential cross section as function of pion scattering angle at three pion kinetic energies of 400 MeV, 500 MeV and 662.7 MeV scaled respectively by factors 1000, 10 and 0.1 [39, 40]. The blue bands are obtained using the Glauber model for $\alpha_{\pi N} = 0.9-1.4$ and dashed lines are the calculations of the Berger-Sehgal model [13].

It is shown that the values of $\alpha_{\pi N}$ in the range 0.9 to 1.4 give a very good description of all the available data. We also compare the calculations with the Berger-Sehgal model which gives reasonable description at lower scattering angles only. These values of $\alpha_{\pi N}$ are then used to calculate the band of pion production cross section in neutrino nucleus interactions.

The nuclear density function for lighter nuclei with nuclear mass upto ^{16}O are taken as the harmonic oscillator type as given by

$$\rho(r) = \rho_0 \left(1 + \alpha \frac{r^2}{a^2}\right) \exp\left(-\frac{r^2}{a^2}\right), \quad \rho_0 = \frac{1}{(1 + 1.5\alpha)(\sqrt{\pi} a)^3}. \quad (7)$$

where a and α are given in Table 1. For light composite material $^{13.8}\text{CH}$, we use harmonic oscillator type density with the value of $a = 1.729$ fm (Same as that for ^{14}N) and $\alpha = 1.024$ calculated using formula given in Ref. [41].

For nuclei heavier than ^{16}O , the nuclear density function is taken as two-parameter Fermi (2pF) type function as given by

$$\rho(r) = \frac{\rho_0}{1 + \exp\left(\frac{r-c}{d}\right)}, \quad \rho_0 = \frac{3}{4\pi c^3 \left(1 + \frac{\pi^2 d^2}{c^2}\right)}. \quad (8)$$

Here d is the diffuseness and c is the half value radius in terms of rms radius R_{rms} as $c = \sqrt{(5R_{\text{rms}}^2 - 7\pi^2 d^2)/3}$ using the given average mass number A . For the composite targets with $A_{\text{eff}} > 16$, the R_{rms} is calculated by $R_{\text{rms}} = 0.891A^{1/3}(1 + 1.565A^{-2/3} - 1.043A^{-4/3})$ [42] with $d = 0.537$ fm. Table 1 shows the nuclear density function parameters for Harmonic oscillator [41] and 2pF [43] for various nuclei used in the present work.

Table 1: Nuclear density function parameters for Harmonic oscillator [41] and 2pF [43] density functions for various nuclei.

Nuclear density parameters					
Harmonic oscillator			2pF		
Nucleus	a (fm)	α	Nucleus	c (fm)	d (fm)
${}^7\text{Li}$	1.77	0.329	${}^{28}\text{Si}$	3.14	0.537
${}^{12}\text{C}$	1.687	1.029	${}^{40}\text{Ar}$	3.53	0.542
${}^{16}\text{O}$	1.805	1.446	${}^{56}\text{Fe}$	4.106	0.519
			${}^{207}\text{Pb}$	6.62	0.546

3. Results and discussions

In this section, we present the results of cross sections calculated using Eq. 1 for both neutrino and anti-neutrino interactions with nucleus. The differential cross section corresponding to an experiment is obtained by averaging cross section over all energies weighted by the neutrino (anti-neutrino) energy spectrum for the experiment.

$$\langle \frac{d\sigma}{dQ^2} \rangle = \frac{\int_{E_{\min}}^{E_{\max}} \frac{d\sigma}{dQ^2}(E) \phi(E) dE}{\int_{E_{\min}}^{E_{\max}} \phi(E) dE}. \quad (9)$$

Figure 5 (a) shows the differential cross section $d\sigma/dQ^2$ (averaged over neutrino flux) for the charge current coherent pion production in neutrino-carbon interaction as a function of the square of four-momentum transfer Q^2 and Figure 5 (b) shows the same for anti-neutrino-carbon interaction using the Glauber model based present approach and BS approach. The band in the Glauber model corresponds to the maximum difference due to variation of both $\alpha_{\pi N}$ (in range 0.9-1.4) and ξ (in range 1-2) while for BS model the band includes variation of ξ only. The calculations correspond to the average energy 4.5 GeV for neutrinos and 4 GeV for anti-neutrinos for the case of MINER ν A experiment [21]. The Glauber approach gives a better agreement (as compared to BS) with the data especially at high Q^2 .

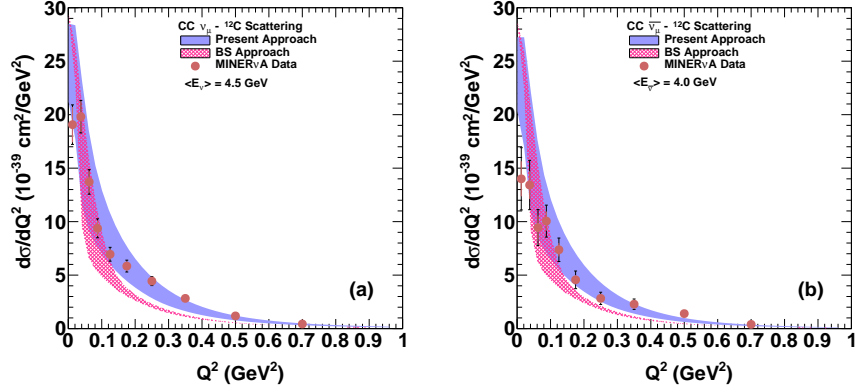


Figure 5: Differential cross section $d\sigma/dQ^2$ (averaged over neutrino and anti-neutrino flux) for the charge current coherent pion production in $\nu_\mu - {}^{12}\text{C}$ interaction as a function of the square of four-momentum transfer Q^2 obtained using the Glauber model based present approach and BS approach for (a) neutrinos with $\langle E_\nu \rangle = 4.5$ GeV and (b) anti-neutrinos with $\langle E_{\bar{\nu}} \rangle = 4$ GeV in comparison with MINER ν A data [21].

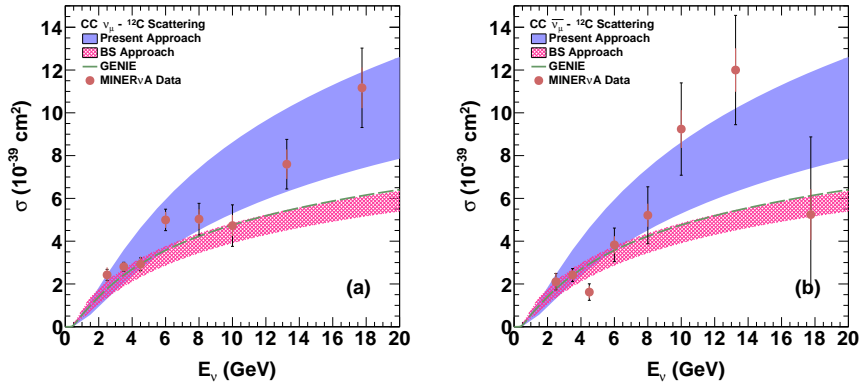


Figure 6: Total cross section σ for the charge current coherent pion production in $\nu_\mu - {}^{12}\text{C}$ interaction as a function of neutrino energy E_ν obtained using the Glauber model based present approach and BS approach for (a) neutrinos and (b) anti-neutrinos. The calculations are compared with the MINER ν A data [21] and GENIE.

Figure 6 (a) shows the total cross section for the charge current coherent pion production in neutrino-carbon interaction as a function of neutrino energy and Figure 6 (b) shows the same for anti-neutrino obtained using the Glauber model based present approach and BS approach. The band in the Glauber model corresponds to the maximum difference due to variation of both $\alpha_{\pi N}$ (in range 0.9-1.4) and ξ (in range 1-2) while for BS model, the band includes variation of ξ only. The calculations are compared with the measured data of MINER ν A experiment [21] and GENIE calculations. The present calculations and GENIE give a good description of the data at low energies while at high energies, the present calculation is in better agreement with data as compared to BS approach and GENIE.

The GENIE package uses Rein sehgal (RS) model. The BS model is actually RS model with improvement in the parametrization of the pion nucleon data. The difference between BS approach and GENIE can arise due to the differences between the treatment of pion nucleon data. We have shown the comparison between Berger Sehgal (BS) model and Glauber model in Figs. 2, 3 and 4. The pion nucleus cross section goes as input in PCAC calculations and creates the differences among the neutrino nucleus cross section. The same parameters and input pion nucleon cross sections used for Glauber model are used in BS calculations here and thus the difference between the two is only due to method of the modeling. It looks that the BS model underestimates the pion nucleus cross section at higher energies. The Glauber model has assumptions which work better at higher collision energies.

Figure 7 shows the total cross section for the charge current coherent pion production neutrino (anti-neutrino)-carbon interaction as a function of neutrino energy obtained using the Glauber model based present approach with $\alpha_{\pi N} = 1.1$ and $\xi = 1$. The calculations are done for four different values of axial mass parameter m_A and are compared with MINER ν A experimental data [21]. Different values of m_A make difference only at high energies where there are large uncertainties of the measurements. We have chosen $m_A = 1.05 \text{ GeV}/c^2$ in all our calculations.

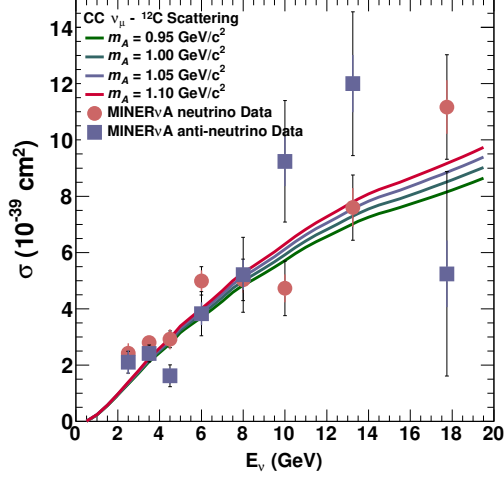


Figure 7: Total cross section σ for the charge current coherent pion production in ν_μ or $\bar{\nu}_\mu - {}^{12}\text{C}$ interaction as a function of neutrino energy E_ν obtained using our calculations ($\alpha_{\pi N} = 1.1$ and $\xi=1$) for four different values of axial mass parameter m_A in comparison with MINERvA experimental data [21].

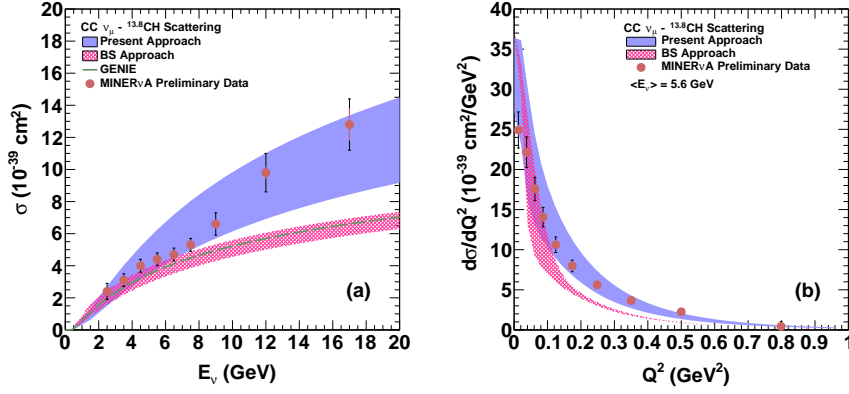


Figure 8: Charge current coherent pion production in $\nu_\mu - {}^{13.8}\text{CH}$ interaction obtained using the Glauber model based present approach and BS approach (a) Total cross section σ as a function of neutrino energy E_ν compared with the preliminary MINERvA data [22] and GENIE and (b) Differential cross section (averaged over neutrino flux [22]) as a function of the square of four-momentum transfer Q^2 compared with the preliminary MINERvA data [22].

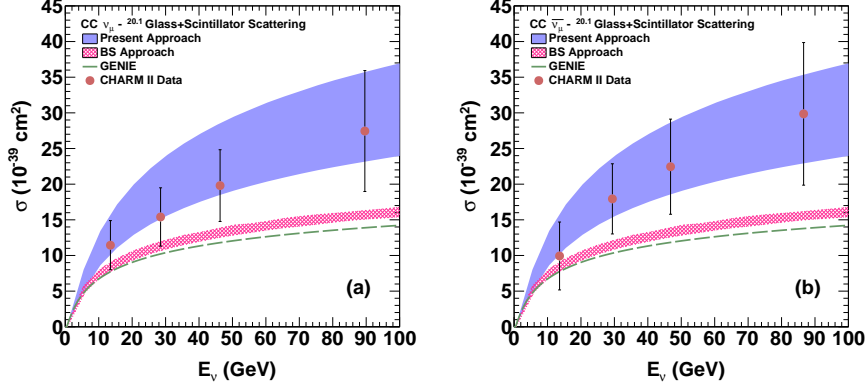


Figure 9: Total cross section σ for the charge current coherent pion production in neutrino-^{20.1}Glass+Scintillator interaction as a function of neutrino energy E_ν obtained using the Glauber model based present approach and BS approach for (a) neutrino and (b) anti-neutrino. The calculations are compared with the CHARM-II data [23] and GENIE.

Figure 8 (a) shows the total cross section for the charge current coherent pion production in neutrino-hydrocarbon interaction as a function of neutrino energy obtained using the Glauber model based present approach and BS approach compared with the preliminary data of MINER ν A experiment [22] and GENIE calculations. Figure 8 (b) shows differential cross section (averaged over neutrino flux [22]) as a function of the square of four-momentum transfer Q^2 obtained using the Glauber model based present approach and BS approach compared with the preliminary data of MINER ν A experiment [22]. The present calculations and GENIE give good description of the total cross section data at low energies while at high energies our calculation is in better agreement with data as compared to GENIE and BS approach. The present calculations of the differential cross section match much better with the data over whole Q^2 range as compared to BS approach. The cross section by GENIE shown in the figure is obtained by scaling their result on carbon with $(13.8/12)^{\frac{2}{3}}$.

Figure 9 (a) shows the total cross section for the charge current coherent pion production in neutrino-glass+scintillator interaction as a function of neutrino energy obtained using the Glauber model based present approach and BS

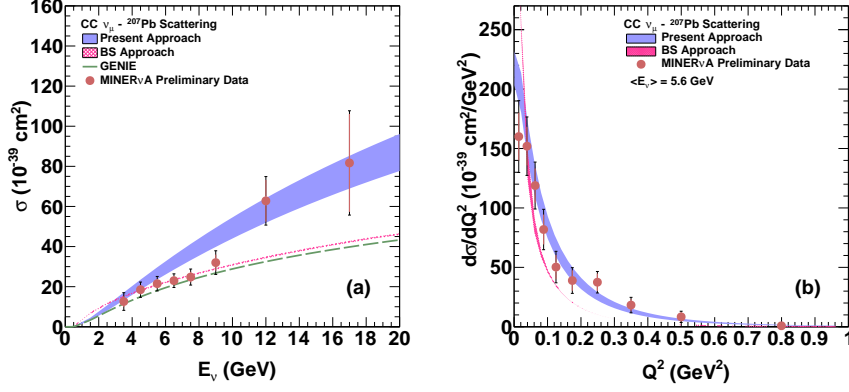


Figure 10: Charge current coherent pion production in ν_μ - ^{207}Pb interaction obtained using the Glauber model based present approach and BS approach compared with the MINERνA data [22] and GENIE. (a) Total cross section σ as a function of neutrino energy and (b) Differential cross section (averaged over neutrino flux) as a function of the square of four-momentum transfer Q^2 [22] compared with the MINERνA data [22].

approach. Figure 9 (b) shows the same for anti-neutrino. The calculations are compared with the measured data of CHARM-II experiment [23] and GENIE. The present calculations are in better agreement with data within experimental error as compared to GENIE and BS approach.

Figure 10 (a) shows the total cross section for the charge current coherent pion production in neutrino-lead interaction as a function of neutrino energy obtained using the Glauber model based present approach and BS approach compared with the measured data of MINERνA experiment [22] and GENIE calculations. Figure 10 (b) shows differential cross section (averaged over neutrino flux [22]) as a function of the square of four-momentum transfer Q^2 compared with the measured data of MINERνA experiment [22]. The present calculations and GENIE give a good description of the total cross section at low energies while at high energies our calculation is in better agreement with data as compared to GENIE and BS model. The present calculations of the differential cross section match much better with the data over whole Q^2 range as compared to BS approach.

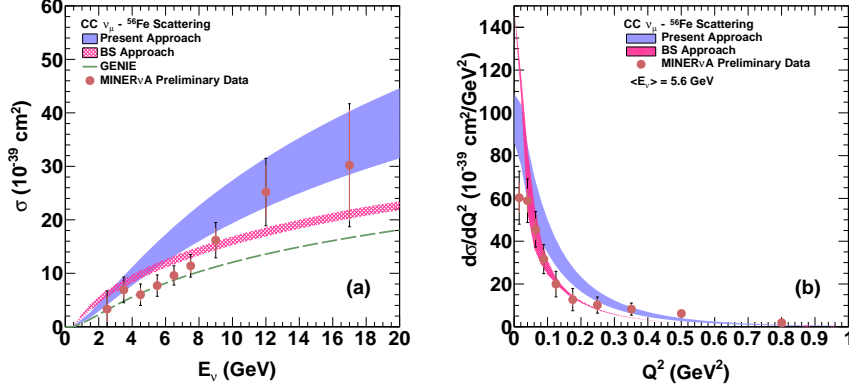


Figure 11: Charge current coherent pion production in $\nu_\mu - {}^{56}\text{Fe}$ interaction obtained using the Glauber model based present approach and BS approach (a) Total cross section σ as a function of neutrino energy are compared with MINER ν A data [22] and GENIE. (b) Differential cross section (averaged over neutrino flux) as a function of the square of four-momentum transfer Q^2 are compared with the MINER ν A data [22].

Figure 11 (a) shows the total cross section for the charge current coherent pion production in neutrino-iron interaction as a function of neutrino energy obtained using the Glauber model based present approach and BS approach compared with the data of MINER ν A experiment [22] and GENIE. This result is relevant for INO as well. Figure 11 (b) shows differential cross section (averaged over neutrino flux) as a function of the square of four-momentum transfer Q^2 [22] compared with the data of MINER ν A experiment [22]. The GENIE and BS give a good description of the data at lower energies while our calculations give reasonable description in the whole energy range.

Figure 12 (a) shows the total cross section prediction for the neutral current coherent pion production in neutrino-iron interaction relevant for INO as a function of neutrino energy obtained using the Glauber model based present approach and BS approach. The calculations are compared with GENIE. Figure 12

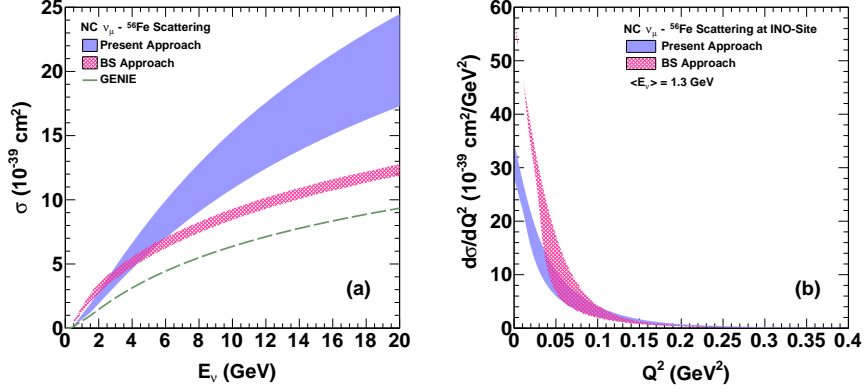


Figure 12: Neutral current coherent pion production in $\nu_\mu-^{56}\text{Fe}$ interaction obtained using the Glauber model based present approach and BS approach (a) Total cross section σ as a function of neutrino energy compared with GENIE and (b) Differential cross section (averaged over neutrino flux at INO-site [4] for solar minimum [44]) as a function of the square of four-momentum transfer Q^2 .

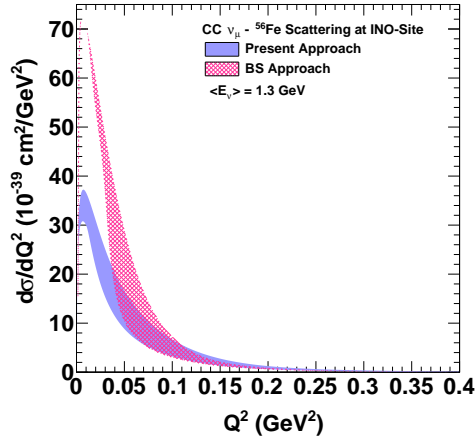


Figure 13: Charge current coherent pion production in $\nu_\mu-^{56}\text{Fe}$ interaction obtained using the Glauber model based present approach and BS approach for differential cross section (averaged over neutrino flux at INO-site for solar minimum [44]) as a function of the square of four-momentum transfer Q^2 .

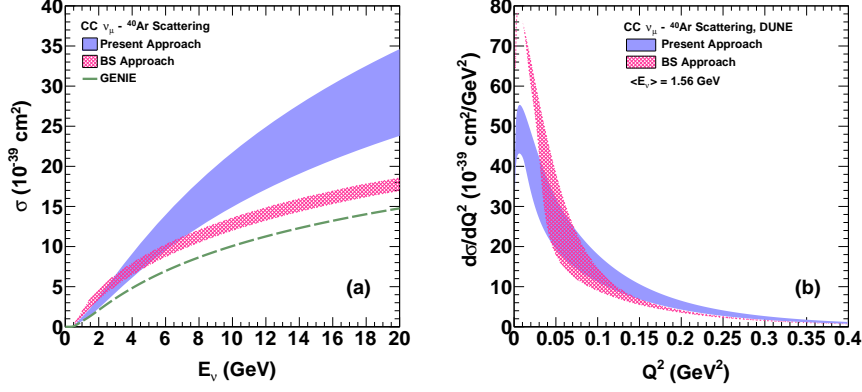


Figure 14: Charge current coherent pion production in $\nu_\mu - {}^{40}\text{Ar}$ interaction obtained using the Glauber model based present approach and BS approach (a) Total cross section predictions as a function of neutrino energy compared with GENIE (b) Differential cross section (averaged over neutrino flux corresponding to the DUNE experiment [5]) as a function of the square of four-momentum transfer Q^2 .

(b) shows differential cross section (averaged over neutrino flux at INO-site [4] for solar minimum from 1 GeV to 20 GeV energy range [44]) as a function of the square of four-momentum transfer Q^2 calculated using Glauber based approach and BS approach.

Figure 13 shows differential cross section for charge current coherent pion production in neutrino-iron interaction as a function of the square of four-momentum transfer Q^2 (averaged over neutrino flux at INO-site for solar minimum from 1 GeV to 20 GeV energy range [44]) calculated using Glauber based approach and BS approach.

Figure 14 (a) shows the total cross section for the charge current coherent pion production in neutrino-argon interaction as a function of neutrino energy obtained using the Glauber model based present approach and BS approach as prediction for the DUNE experiment. The calculations are compared with GENIE. Figure 14 (b) shows differential cross section(averaged over neutrino flux corresponding to the DUNE experiment [5]) as a function of the square of four-momentum transfer Q^2 calculated using Glauber based approach and BS

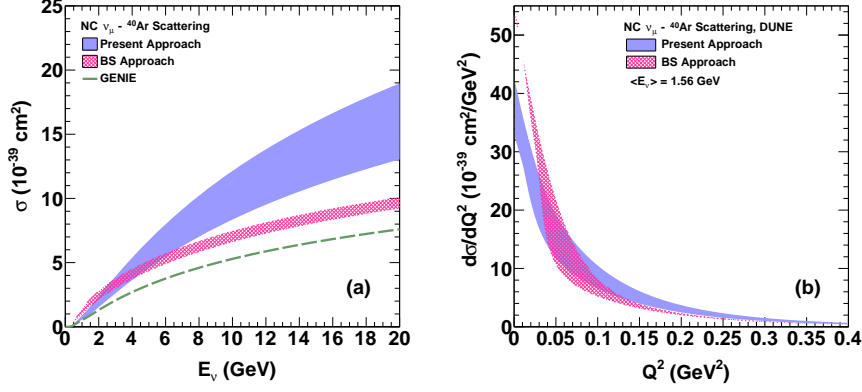


Figure 15: Neutral current coherent pion production in $\nu_\mu-^{40}\text{Ar}$ interaction obtained using the Glauber model based present approach and BS approach (a) Total cross section σ as a function of neutrino energy are compared with GENIE (b) Differential cross section (averaged over neutrino flux corresponding to the DUNE experiment [5]) as a function of the square of four-momentum transfer Q^2 .

approach.

Figure 15 (a) shows the total cross section for the neutral current coherent pion production in neutrino-argon interaction as a function of neutrino energy obtained using the Glauber model based present approach and BS approach as predictions for the DUNE experiment. The calculations are compared with GENIE. Figure 15 (b) shows differential cross section (averaged over neutrino flux corresponding to the DUNE experiment [5]) as a function of the square of four-momentum transfer Q^2 calculated using the Glauber model based present approach and BS approach.

Figure 16 shows the total cross section for the neutral current coherent pion production in neutrino-nucleus interaction as a function of target nucleus mass (^7Li , ^{12}C , ^{16}O , ^{28}Si , ^{40}Ar and ^{56}Fe) obtained using the Glauber model based present approach. The calculations are compared with BS approach, GENIE and experiments: Aachen-Padova [24], Gargamelle [25], CHARM [26], SKAT [27], NOMAD [28], 15'B.C. [29] and SciBooNE [30]. The calculations give a very good description for several experimental data for a wide range of

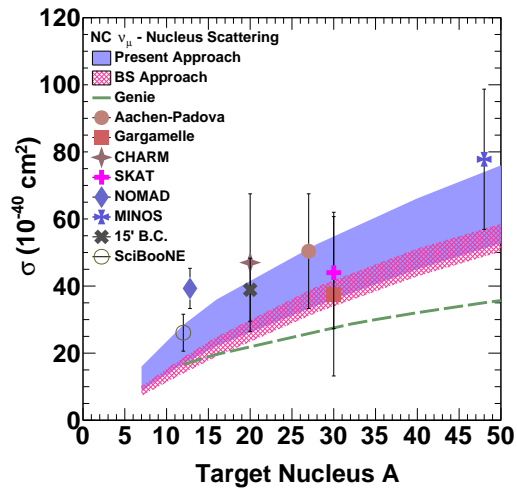


Figure 16: Total cross section σ for the neutral current coherent pion production in ν_μ -nucleus interaction as a function of nuclear mass A at 4.9 GeV neutrino energy obtained using the Glauber model based present approach. The measurements of experiments are scaled to $E_\nu = 4.9$ GeV [31] using the Berger-Sehgal [13] approach. The results obtained using our calculations are compared with BS approach, GENIE and experiments: Aachen-Padova [24], Gargamelle [25], CHARM [26], SKAT [27], NOMAD [28], 15'B.C. [29] and SciBooNE [30]

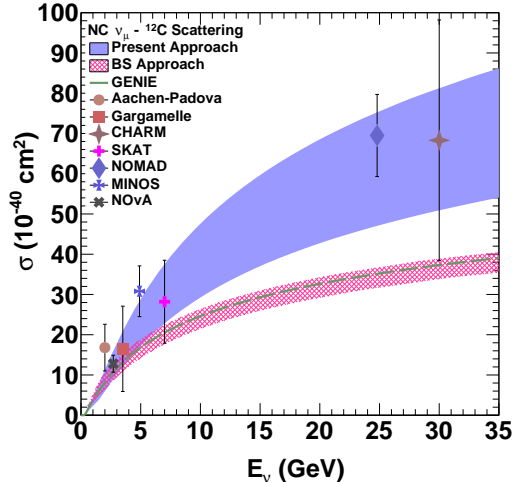


Figure 17: Total cross section σ for the neutral current coherent pion production in $\nu_\mu-^{12}\text{C}$ interaction as a function of neutrino energy. The cross sections obtained using the Glauber model based present approach and BS approach are compared with GENIE and experiments: Aachen-Padova [24], Gargamelle [25], CHARM [26], SKAT [27], NOMAD [28], MINOS [31] and NO ν A [32]. The cross section measurements of experiments with different nuclei of mass number A are scaled to carbon [31] using $(12/A)^{\frac{2}{3}}$.

targets and are much better than GENIE. The measurements of experiments are scaled to $E_\nu = 4.9$ GeV [31] using the Berger-Sehgal [13] approach.

Figure 17 shows the total cross section for the neutral current coherent pion production in neutrino-carbon interaction as a function of neutrino energy obtained using the Glauber model based present approach and BS approach. The calculations are compared with GENIE and experiments: Aachen-Padova [24], Gargamelle [25], CHARM [26], SKAT [27], NOMAD [28], MINOS [31] and NO ν A [32]. The Glauber based calculations give a very good description for experimental data in a wide range of energy. GENIE and BS approach give a good description of data only at low neutrino energies. The cross section measurements of experiments with different nuclei of mass number A are scaled to carbon [31] using $(12/A)^{\frac{2}{3}}$.

Table 2: Comparison of the calculated total cross sections σ for coherent pion production using Glauber and BS approach with the measurements by different experiments along with the average energy of neutrinos.

Exps.	$\langle A \rangle$	Current, particle	$\langle E \rangle$ GeV	σ (10^{-39}cm^2)		
				Glauber	BS	Exp.
SKAT [27]	30	CC, ν	7	8.8-13.3	7.7-9.2	10.6 ± 1.6
SKAT [27]	30	CC, $\bar{\nu}$	7	8.8-13.3	7.7-9.2	11.3 ± 3.5
SKAT [27]	30	NC, ν	7	5.0-7.5	4.3-5.1	5.2 ± 1.9
MINOS [31]	48	NC, ν	4.9	5.1-7.3	4.9-5.7	3.26 ± 0.21
NO ν A [32]	13.8	NC, ν	2.7	1.0-1.8	1.0-1.5	1.4 ± 0.2

Table 2 shows a comparison of the calculated total cross sections σ for coherent pion production using Glauber and BS approach with the measurements by different experiments SKAT [27], MINOS [31] and NO ν A [32] along with the average energy of neutrinos. In the SKAT experiment, target material is Heavy freon ($A = 30$) and the calculation is done on the average energy of neutrinos in the experiment. In the MINOS experiment, target material is the composition of 80% iron and 20% carbon ($A = 48$). The cross section is averaged over the flux. In the NO ν A experiment target material is mainly the composition of 66.7% carbon, 16.1% chlorine and 10.8% hydrogen and other nuclei ($A = 13.8$). The table shows excellent agreement between the data and the calculations, especially at higher energy.

4. Conclusions

In this work, we presented a comprehensive study of coherent pion production in neutrino-nucleus interactions in the resonance region using the formalism based on PCAC theorem. Pion-nucleus elastic scattering cross section is calculated using the Glauber model which takes three inputs, nuclear densities, pion-nucleon cross section and $\alpha_{\pi N}$ for which the parametrizations are obtained

from measured data. We obtain the differential and integrated cross sections for charge and neutral current coherent pion production in neutrino (anti-neutrino)-nucleus scattering for a range of targets such as lithium, carbon, hydrocarbon, scintillator, oxygen, silicon, argon, iron and lead. The results of these cross section calculations are compared with the measured data, BS model and GENIE package. There is an excellent agreement between the calculated cross section from Glauber model and measured cross sections. Predictions are also made for upcoming experiments like INO and DUNE in the coherent pion production region of the neutrino cross section.

Acknowledgements We thank Dr. Kapil Saraswat for many fruitful discussions during the course of this work.

References

- [1] M. D. Messier, eConf **C060409** (2006), 018 [arXiv:hep-ex/0606013 [hep-ex]].
- [2] M. V. Diwan, V. Galymov, X. Qian and A. Rubbia, Ann. Rev. Nucl. Part. Sci. **66**, 47 (2016). [arXiv:1608.06237 [hep-ex]].
- [3] P. A. Zyla *et al.* [Particle Data Group], PTEP **2020**, 083C01 (2020)
- [4] S. Ahmed *et al.* [ICAL], Pramana **88**, 79 (2017).
- [5] B. Abi *et al.* [DUNE], Eur. Phys. J. C **80**, 978 (2020).
- [6] J. A. Formaggio and G. P. Zeller, Rev. Mod. Phys. **84**, 1307 (2012).
- [7] K. Saraswat, P. Shukla, V. Kumar and V. Singh, Indian J. Phys. **92**, 249 (2018)
- [8] D. Grover, K. Saraswat, P. Shukla and V. Singh, Phys. Rev. C **98**, 065503 (2018), [arXiv:1808.00287 [hep-ph]].
- [9] D. Rein and L. M. Sehgal, Nucl. Phys. B **223**, 29 (1983).
- [10] B. Z. Kopeliovich and P. Marage, Int. J. Mod. Phys. A **8**, 1513 (1993).
- [11] B. Z. Kopeliovich, Nucl. Phys. Proc. Suppl. **139**, 219 (2005).
- [12] A. Kartavtsev, E. A. Paschos, and G. J. Gounaris, Phys. Rev. D **74**, 054007 (2006).
- [13] C. Berger and L. M. Sehgal, Phys. Rev. D **79**, 053003 (2009).
- [14] E. A. Paschos and D. Schalla, Phys. Rev. D **80**, 033005 (2009).
- [15] S. K. Singh, M. S. Athar and S. Ahmad, Phys. Rev. Lett. **96**, 241801 (2006).
- [16] L. Alvarez-Ruso, L. S. Geng, S. Hirenzaki and M. J. Vicente Vacas, Phys. Rev. C **75**, 055501 (2007). Phys. Rev. C **80**, 019906 (2009).

- [17] L. Alvarez-Ruso, L. S. Geng and M. J. Vicente Vacas, Phys. Rev. C **76**, 068501 (2007), [Phys. Rev. C **80**, 029904 (2009)].
- [18] J. E. Amaro, E. Hernandez, J. Nieves and M. Valverde, Phys. Rev. D **79**, 013002 (2009).
- [19] C. Andreopoulos, A. Bell, D. Bhattacharya, F. Cavanna, J. Dobson, S. Dytman, H. Gallagher, P. Guzowski, R. Hatcher and P. Kehayias, *et al.* Nucl. Instrum. Meth. A **614** (2010), 87-104
- [20] K. Saraswat, P. Shukla, V. Kumar and V. Singh, Phys. Rev. C **93**, 035504 (2016). [arXiv:1602.07820 [hep-ph]].
- [21] A. Mislivec *et al.* [MINERvA], Phys. Rev. D **97**, 032014 (2018).
- [22] Manuel Alejandro Ramirez Delgado, [MINERvA], $\mu\nu$ -induced CC coherent π^+ production off carbon, hydrocarbon, iron, and lead using the MINERVA detector, FERMILAB-THESIS-2020-10 (2020). doi:10.2172/1638645.
- [23] P. Vilain *et al.* [CHARM-II], Phys. Lett. B **313**, 267 (1993).
- [24] H. Faissner *et al.* [Aachen Padova], Phys. Lett. B **125**, 230 (1983).
- [25] E. Isiksal, D. Rein and J. G. Morfin [Gargamelle], Phys. Rev. Lett. **52**, 1096 (1984).
- [26] F. Bergsma *et al.* [CHARM], Phys. Lett. B **157**, 469 (1985).
- [27] H. J. Grabosch *et al.* [SKAT], Z. Phys. C **31**, 203 (1986).
- [28] C. T. Kullenberg *et al.* [NOMAD], Phys. Lett. B **682**, 177 (2009).
- [29] C. Baltay, M. Bregman, D. Caroumbalis, L. D. Chen, M. Hibbs, J. T. Liu, J. Okamitsu, G. Ormazabal, A. C. Schaffer and K. Shastri, *et al.* Phys. Rev. Lett. **57**, 2629 (1986).
- [30] Y. Kurimoto *et al.* [SciBooNE], Phys. Rev. D **81**, 033004 (2010).

- [31] P. Adamson *et al.* [MINOS], Phys. Rev. D **94**, 072006 (2016).
- [32] M. A. Acero *et al.* [NOvA], Phys. Rev. D **102** 012004, (2020); Flux for 2017 analysis, NOVA Document 25266-v3.
- [33] M. H. Ahn *et al.* [K2K], Phys. Rev. D **74**, 072003 (2006).
- [34] K. Abe *et al.* [T2K], Phys. Rev. D **87**, 012001 (2013).
- [35] K. Abe *et al.* [T2K], Phys. Rev. Lett. **117**, 192501 (2016).
- [36] J. L. Raaf, [MiniBooNE], Fermilab-Thesis-2005-20, (2005).
- [37] P. Shukla, “Glauber model for heavy ion collisions from low-energies to high-energies,” arXiv:nucl-th/0112039.
- [38] A. Mehndiratta and P. Shukla, Nucl. Phys. A **961**, 22 (2017), [arXiv:1702.07459 [nucl-th]].
- [39] G. Kahrmanis, *et al.* Phys. Rev. C **55**, 2533 (1997). [arXiv:nucl-ex/9702003 [nucl-ex]].
- [40] D. Marlow, *et al.*, Phys. Rev. C **30**, 1662 (1984).
- [41] C. W. De Jager, H. De Vries and C. De Vries, Atom. Data Nucl. Data Table **14**, 479 (1974).
- [42] Friedrich, J., Voegler, N.: Nucl. Phys. A **373**, 192 (1982);
- [43] H. De Vries, C. W. De Jager and C. De Vries, Atom. Data Nucl. Data Table **36**, 495 (1987).
- [44] M. Honda, M. S. Athar, T. Kajita, K. Kasahara, S. Midorikawa, Phys. Rev. D **92**, 023004 (2015).